Active Contour Models for Extracting Ground and Forest Canopy Curves from Discrete Laser Altimeter Data

Mahmoud Awadallah[1], Sherin Ghannam[1], Lynn Abbott[1], and Ahmed Ghanem[2]

[1]Bradley Department of Electrical and Computer Engineering, Virginia Tech, Blacksburg, Virginia, USA, {mawadallah,sghannam,abbott}@vt.edu

[2]Electrical Engineering Department, Suez Canal University, Ismailia, Egypt, ghanem@gmail.com

Paper Number: SL2013-033

1. Introduction

The importance of finding efficient ways of quantifying terrestrial carbon stocks at a global scale has increased due to the concerns about global climate change. Exchange of carbon between forests and the atmosphere is a vital component of the global carbon cycle (Nelson et al. 2003). Recent advances in remote sensing technology have facilitated rapid and inexpensive measurements of topography over large areas (Zhang et al. 2003).

Lidar (light detection and ranging) has been studied since the 1960s (Flood 2001; Liu 2008). Airborne lidar for topographic data collection was developed in the 1980s (Krabill et al. 1984; Bufton et al. 1991), and commercial airborne lidar systems have been operational since the mid-1990s (Pfeifer and Briese 2007). There has been a significant increase in the use of lidar data for Digital Elevation Model (DEM) generation over the last decade as lidar systems have become more reliable, more accurate, and less expensive (Sithole and Vosselman 2003). Kraus and Pfeifer (1998) concluded that the accuracy of lidar-derived DEMs for forested areas is comparable to that of DEMs for open areas obtained using photogrammetric techniques. Various filtering methods have been developed to classify or separate raw lidar data into ground and non-ground data. However, automated filtering techniques are not perfectly accurate (Romano 2004), and manual editing of the filtering results is often needed (Chen 2007; Chen et al. 2007).

This paper presents a novel framework capable of automatically estimating the ground and top of canopy (TOC) from noisy high-altitude lidar data. This framework utilizes the technique of active contour models in making this estimation. The rest of the paper is organized as follows. The methodology and main contribution of the paper are presented in section 2. Section 3 describes the results that we have obtained. Finally, section 4 concludes the paper.

2. Methodology

The main contribution of this paper is to introduce the development of a novel framework based on active contour models (often called deformable models or “snakes”) to estimate ground and TOC from discrete LIDAR data. The proposed framework is summarized in Figure 1. Active contours are expressed as an energy minimization process (Kass et al. 1988), and they rely on higher level mechanisms to place them near a desired solution. The framework presented here proposes an automatic procedure to discover a region of interest (ROI) to initialize the location of the snakes near ground and TOC. A good selection of ROI helps prevent the attraction of snakes to incorrect solutions, and can improve computation speed by reducing the number of iterations required to converge. This paper describes an open-curve snake algorithm that has efficiently located ground and TOC in some experiments, as well as a closed-curve snake algorithm that has produced results with higher accuracy.

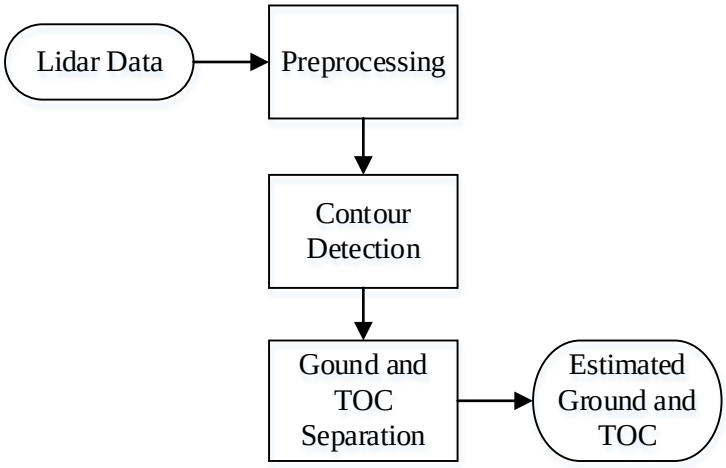

Figure 1: Overview of system. The goal is to detect curves that correspond to the ground and to the top of the canopy (TOC).

2.1 Lidar data

Lidar sensing produces a set of three-dimensional (3D) points, where each point is represented by coordinates (*x*, *y*, *z*). In order to apply image processing techniques, our first step is to map these points onto a two-dimensional (2D) binary image. An example is given in Figure 2(a).

2.2 Preprocessing

A preprocessing step is needed to reduce noise in the image, and to provide an initial estimate for the optimization routine. This step is essential for avoiding incorrect results. In our current implementation, the system applies a median filter which dramatically reduces noise as shown in Figure 2(b). This filter is followed by a size filter which removes small isolated regions that may exist after the median filter (Figure 2(c)).

2.3 Contour detection

Active contours are typically implemented using an energy minimization process (Kass et al. 1988). Given an initial curve v in the image, the curve is transformed through repeated steps that attempt to minimize an energy functional E_{snake}. The name "snake" results from the appearance of the curve v as it changes during the iterative process.

The energy functional is commonly defined using several additive terms, such as the following:

$$E_{snake} = \int_0^1 [E_{int}(v(s)) + E_{image}(v(s)) + E_{con}(v(s))]ds \quad (1)$$

An "internal" energy term E_{int} affects the degree to which the contour can bend and stretch. An "external" energy term E_{image} incorporates effects from image properties, such as magnitudes of intensity edges, and a second external energy term E_{con} may specify additional constraints. In this way, a snake represents a compromise between the curve's own properties (such as curvature) and image properties (such as contrast or texture).

In our implementation, the internal image energy is defined as follows:

$$E_{int} = \alpha(s)\left|\frac{dv(s)}{ds}\right|^2 + \beta(s)\left|\frac{d^2v(s)}{ds^2}\right|^2 \quad (2)$$

The first-order term represents the energy due to stretching (elastic energy), and the second-order term measures the energy due to bending (curvature energy). The image energy attracts the snake to low-level features in the image. The original formulation suggested that lines, edges and terminations could contribute to the energy function, as follows:

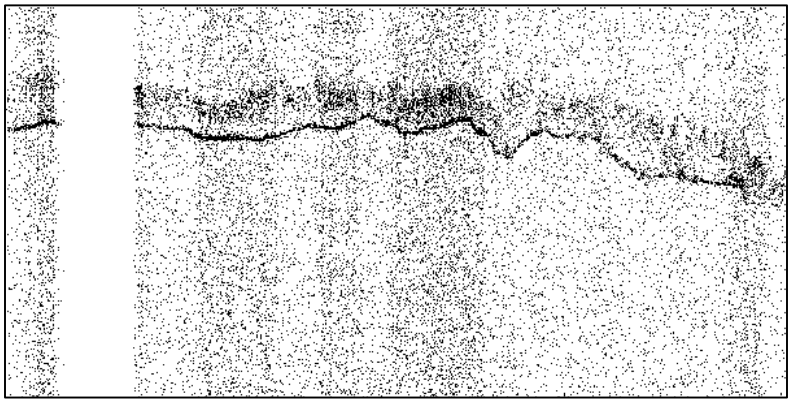

(a)

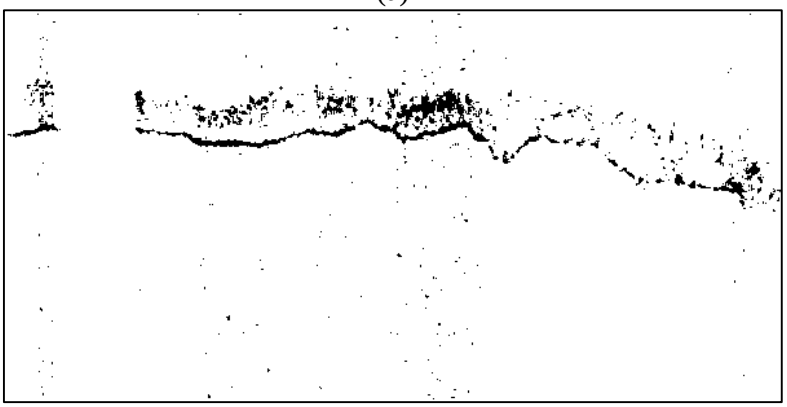

(b)

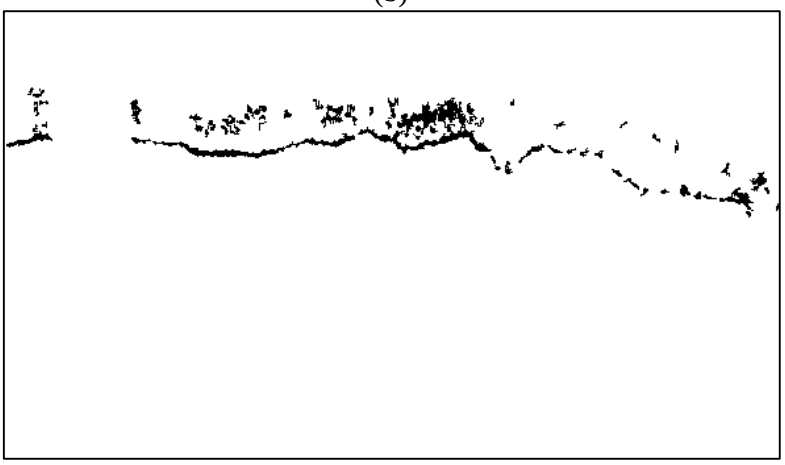

(c)

Figure 2: Example of noise reduction steps. (a) Original lidar data. Each dark point represents a single lidar measurement. (b) Result of median filter. (c) Result of size filter. For this example, the points that remain are near the ground and vegetation.

$$E_{image} = w_{line} E_{line} + w_{edge} E_{edge} + w_{term} E_{term} \quad (3)$$

A greedy algorithm can be used to search for a solution (Williams and Shah 1992). The process starts by specifying an initial contour, and then the snake evolves in an iterative manner by local neighborhood search around contour points to select new points that have lower overall energy.

The framework proposed in this paper adapts this greedy approach for estimation of ground and TOC contours, with satisfactory results. The first algorithm starts with two snakes, one near the top of the image, and one near the bottom. External constraints force the first snake to move only downward in the image, and the second snake to move only upward. Other constraints keep the leftmost and rightmost points of both snakes at the image boundaries, and also keep the internal points evenly spaced. This approach produced good results with a very fast convergence and efficient calculations. However, this approach is necessarily very sensitive to noise, so the preprocessing step is crucial. One of the major drawbacks of the median filter is that it may remove some important data points leading to inaccurate estimations in many cases. Also, this approach did not converge well near sharp concavities, such as those caused by gaps in the canopy where no trees are present.

The proposed solution to these problems has been to consider another snake algorithm that is more robust against noise, and is capable of handling concavities, sharp corners and background contamination that may present in the image. This approach is known as a *geometric active contour* (GAC) model, and the associated curve is represented implicitly using a level-set function. Chan and Vese (2001) introduced a GAC that is based on the Mumford-Shah functional (Mumford and Shah 1989). Their model uses regional image statistics for segmentation, and as a result it is sometimes called a *region-based* level-set model.

The lidar data in the proposed framework can be interpreted as a bimodal image I_0 that contains a single object of interest (vegetation plus ground) against a noisy but fairly regular background. Although our images are binary, we can consider the object and background to have pixels of average intensity levels c_1 and c_2, respectively. Then the goal can be formulated as a search for a closed curve C within the image such that all object pixels are inside the curve, and all background pixels are outside the curve. A new energy term can be written as

$$E(C) = \int_{inside(C)} |I_0(x,y) - c_1|^2 dxdy + \int_{outside(C)} |I_0(x,y) - c_2|^2 dxdy \quad (4)$$

Ideally, the above equation is minimized when the contour C is coincident with the boundary of the foreground object in the image. Let $\psi(x, y)$ represent the signed Euclidean distance of an image point (x, y) from the curve C:

$$\psi(x,y) = \begin{cases} 0 & if\ (x,y) \text{ is on the curve} \\ <0 & if\ (x,y) \text{ is inside the curve} \\ >0 & if\ (x,y) \text{ is outside the curve} \end{cases} \quad (5)$$

The function ψ is therefore an implicit representation of the curve C, and is called the embedding function for C. An evolution equation is given by

$$\frac{\partial \psi}{\partial t} = [\mu\, div(\frac{\nabla \psi}{|\nabla \psi|}) - (\lambda_1 (I_0 - c_1)^2 + \lambda_2 (I_0 - c_2)^2)] \quad (6)$$

where λ_1, λ_2, and μ are constants. The first term, $div(\frac{\nabla\psi}{|\nabla\psi|})$, represents the curvature of C and is calculated as

$$div(\frac{\nabla\psi}{|\nabla\psi|}) = -\frac{\psi_{xx}\psi_y^2 - 2\psi_x\psi_y\psi_{xy} + \psi_{yy}\psi_x^2}{(\psi_x^2 + \psi_y^2)^{3/2}} \quad (7)$$

The second term of (6), the model-fit error term, drives the evolution of the contour. This error term is minimized when the contour perfectly subdivides the image in such a way that the average intensities inside and outside the contour perfectly match the constants c_1 and c_2, respectively.

An advantage of this approach is that strong intensity edges between foreground and background are not necessary for successful operation. However, this algorithm is again very sensitive to the initial location of the contours. A proposed solution to this problem is to use median and size filters as a method to estimate the ROI as a good initialization. This technique has led to good results in our experiments.

2.4 Ground and top-of-canopy separation

After detecting contours as described in the previous sections, the last stage is discriminating ground and TOC from the resultant contours. This task is straightforward in the open-curve approach, because the upper snake is assumed to lie on the TOC while the lower snake tracks the ground. However, for the GAC approach this step is a little trickier because the output of the snake procedure is a closed contour, or possibly several closed contours. In our approach, at selected columns of the image, the uppermost points from the contour are assigned to the TOC, and the lowest points from the contour are assigned to the ground. Interpolation is applied for any gaps that result in either curve.

3. Experimental Results

A MATLAB program was implemented to assess the framework explained in this paper. A dataset was obtained from NASA that comprise 15 files of simulated ICESat-2 lidar data (Abdalati et al. 2010). The 15 files represent 5 different flight transects (labeled Cedar-2, Cedar-4, SERC-1, SERC-3 and SERC-5), each on the order of 1.5 to 4 km in length. For each transect, ambient noise was added at 3 different levels, with the noise varying based on target reflectivity. The files designated as “0.5 MHz” simulate nighttime acquisitions, which is when ambient noise is at the lowest level. The other files are designated “2 MHz” and “5 MHz,” representing late daytime acquisitions with clear sky, and daytime acquisitions with a hazy atmosphere, respectively.

Experimental results for some of these files are shown in Figures 3 and 4. For each figure, part (a) shows an example result for the open-curve method, and part (b) shows a result for the closed-curve GAC method. Each of these figures reveals insights for the two approaches. For the open-curve snake approach, a Distance Transform was used, which provided a non-negative value $D(x, y)$ corresponding to the distance from pixel (x, y) to the nearest feature in the image. These values were used in the energy term E_{image} of (1), instead of the more traditional values that depend on intensity-gradient values. From the GAC diagrams, notice that the TOC contours represents gaps in the tree line more accurately than for the open-curve method.

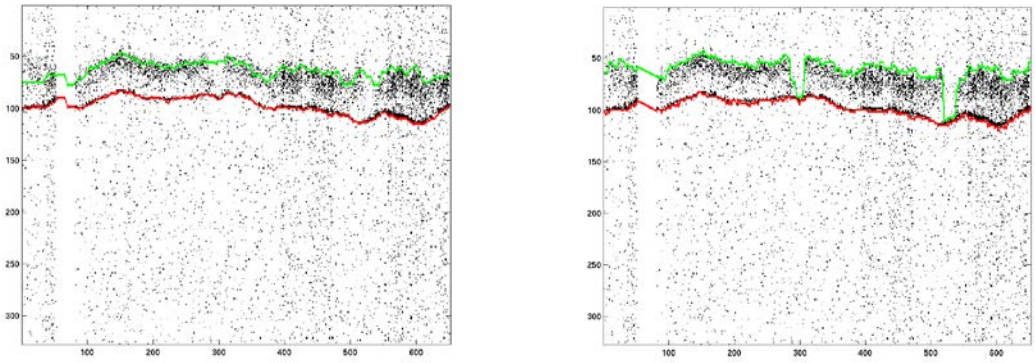

(a) (b)

Figure 3. Comparison between open and closed contour approaches for Cedar-2 data set. (a) Open-curve snake. (b) Closed-curve (region-based) snake.

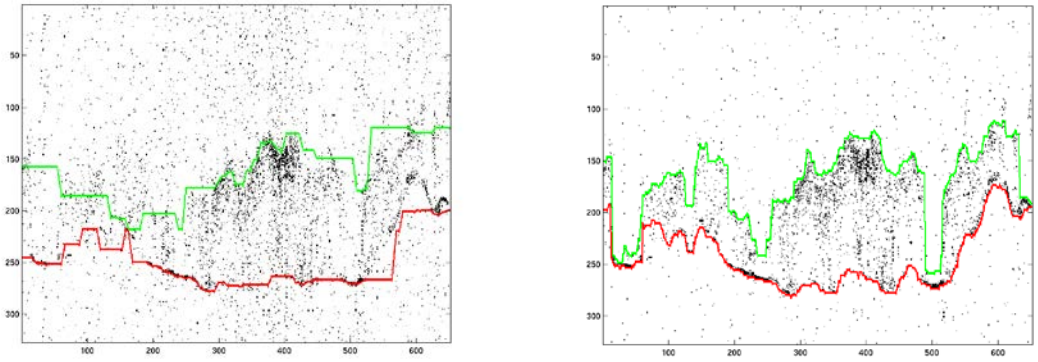

(a) (b)

Figure 4: Comparison between open and closed contour approaches for SERC-3 data set. (a) Open-curve snake. (b) Closed-curve (region-based) snake.

To evaluate the performance of both approaches, the statistical indicators known as *recall* and *precision* were computed. Recall *R* is the fraction of true signal points (according to the provided ground truth) that are successfully enclosed within the contours. Precision *P* is the fraction of true signal points from all the points enclosed within the detected contours. These indicators have been used for evaluation of image-retrieval and image-segmentation techniques (Martin et al. 2004), and are formally defined as

$$R = \frac{TP}{TP + FN}, \qquad P = \frac{TP}{TP + FP} \tag{8}$$

where *TP*, *FP*, and *FN* represent the numbers of true positives, false positives, and false negatives, respectively. In order to use a single performance measure that will allow for comparison of results, the harmonic mean of recall and precision was used, which is commonly referred to as the *F-measure*:

$$F = \frac{2PR}{P + R} \tag{9}$$

Ideal performance correspond to the case that $R = 1$ and $P = 1$, resulting in $F = 1$. Figure 5 shows a comparison between the performances of the two approaches for the given data set. For

practically all of the data sets, the *F*-measure value for the closed-curve snake model is noticeably greater than the *F*-measure value for the open-curve snake. This result can perhaps be explained by the fact that the open-curve approach relies on the distance transform, which is more sensitive to noise. As expected, for both approaches the worst performance was observed for cases with the most severe noise (5 MHz rate). For the other noise levels, the *F*-measure values all exceeded 0.84.

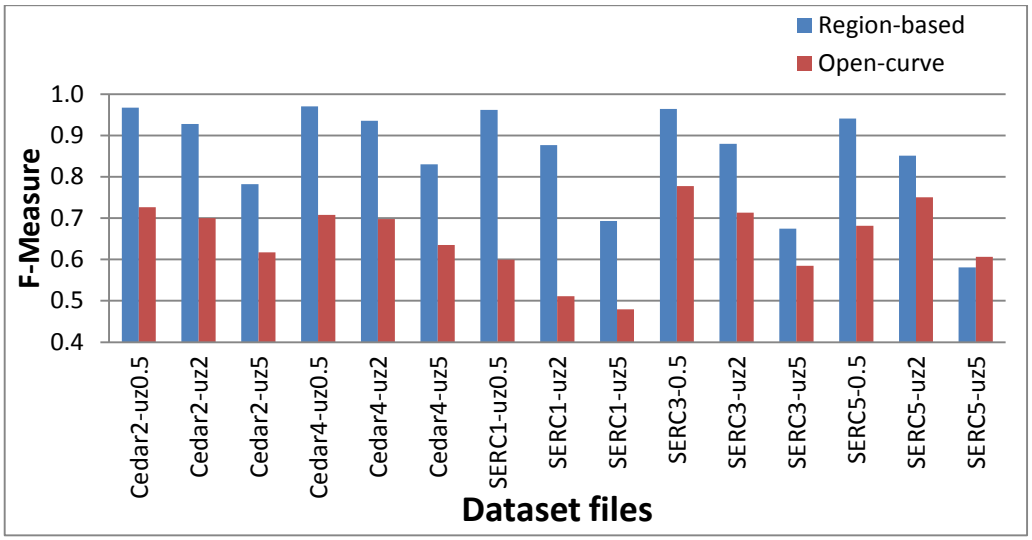

Figure 5: *F*-measure values that were obtained for both approaches. Except for one case at the far right, better results were obtained for the region-based (closed-curve) approach. Slightly different stopping criteria were employed in these experiments.

4. Discussion

This paper has proposed a novel framework capable of automatically estimating ground and top-of-canopy contours within noisy discrete lidar data. The method utilizes techniques based on deformable models, also known as snakes, which are common in the field of image analysis. Two different snake-based approaches were considered here. The open-curve approach, combined with an image-distance transform, achieved reasonable *F*-measure scores in most cases. The closed-curve technique was better in all but one of the test cases, and exhibited an *F*-measure score above 0.84 except at the worst noise level. Whereas deformable models are commonly used with gray-scale and color images, this is one of the first studies involving deformable models for binary images.

Acknowledgements

The authors gratefully acknowledge the datasets and comments from Dr. Ross Nelson at NASA's Goddard Space Flight Center. The authors also thank Dr. Randolph Wynne, Dr. Valerie Thomas, and Mr. Ranjith Gopalakrishnan at Virginia Tech for many helpful discussions.

References

Abdalati, W., Zwally, H., Bindschadler, R., Csatho, B., Farrell, S., Fricker, H., and Webb, C., 2010. The ICESat-2 laser altimetry mission. *Proceedings of the IEEE*, 98 (5), 735-751.

Bufton, J. L., Garvin, J. B., Cavanaugh, J. F., Ramos-lzquierdo, L., Clem, T. D., and Krabill, W. B. 1991. Airborne lidar for profiling of surface topography. *Optical Engineering*, 30, 72-78.

Chan, T., and Vese, L. 2001. Active contours without edges. *IEEE Transactions on Image Processing*, 10 (2), 266-277.

Chen, Q. 2007. Airborne lidar data processing and information extraction. *Photogrammetric Engineering and Remote Sensing*, 73, 109-12.

Chen, Q., Gong, P., Baldocchi, D., and Xin, G. 2007. Filtering airborne laser scanning data with morphological methods. *Photogrammetric Engineering and Remote Sensing*, 73, 175-85.

Martin, D. R., Fowlkes, C. C., and Malik, J. 2004. Learning to detect natural image boundaries using local brightness, color, and texture cues. *IEEE Transactions on Pattern Analysis and Machine Intelligence*, 26 (5), 530-549.

Flood, M. 2001. Laser altimetry - from science to commercial lidar mapping. *Photogrammetric Engineering and Remote Sensing*, 67 (11), 1209-1217.

Kass, M., Witkin, A., and Terzopoulos, D. 1988. Snakes: Active contour models, *International Journal of Computer Vision*, 1 (4), 321-331.

Krabill, W. B., Collins, J. G., Link, L. E., Swift, R. R., and Butler, M. L. 1984. Airborne laser topographic mapping results. *Photogrammetric Engineering and Remote Sensing*, 50, 685-94.

Kraus, K., and Pfeifer, N. 1998. Determination of terrain models in wooded areas with airborne laser scanner data. *ISPRS Journal of Photogrammetry and Remote Sensing*, 53, 193-203.

Liu, X. 2008. Airborne LiDAR for DEM generation: some critical issues. *Progress in Physical Geography*, 32 (1), 31–49.

Mumford, D., and Shah, J. 1989. Optimal approximation by piecewise smooth functions and associated variational problems. *Communications on Pure and Applied Mathematics*, 42, 577-685.

Nelson, R., Valenti, M. A., Short, A., and Keller, C. 2003. A multiple resource inventory of Delaware using airborne laser data. *BioScience*, 53 (10).

Pfeifer, N., and Briese, C. 2007. Geometrical aspects of airborne laser scanning and terrestrial laser scanning. *International Archives of Photogrammetry, Remote Sensing and Spatial Information Sciences*, 36 (3), 311-19.

Romano, M. E. 2004. Innovation in lidar processing technology. *Photogrammetric Engineering and Remote Sensing*, 70, 1202-1206.

Sithole, G., and Vosselman, G. 2003. ISPRS comparison of filters. Technical Report, Department of Geodesy, Faculty of Civil Engineering and Geosciences, Delft University of Technology, The Netherlands.

Williams, D. J., and Shah, M. 1992. A fast algorithm for active contours and curvature estimation. *CVGIP: Image Understanding*, 55 (1), 14-26.

Zhang, K., Chen, S., Whitman, D., Shyu, M., Yan, J., and Zhang, C. 2003. A progressive morphological filter for removing non-ground measurements from airborne lidar data. *IEEE Transactions on Geoscience and Remote Sensing*, 41 (4), 872-882.